Effects of Composition on Crystal Structure, Thermal Expansion, and Response to Pressure in ReO_3-type $MNbF_6$(M= Mn and Zn)

Brett R. Hester,[†] and Angus P. Wilkinson*[,†,§]

[†] School of Chemistry and Biochemistry, Georgia Institute of Technology, Atlanta, GA 30332-0400, United States

[§]School of Materials Science and Engineering, Georgia Institute of Technology, Atlanta, GA 30332-0245, United States

* Corresponding author: angus.wilkinson@chemistry.gatech.edu

ABSTRACT: ReO_3-type ABF_6, are of interest as low and negative thermal expansion (NTE) materials. As only cubic ABF_6 display NTE, the occurrence of phase transitions needs to be understood. The thermal expansion, phase behavior on heating and compression, and compressibilities of $MnNbF_6$ and $ZnNbF_6$ were examined by synchrotron powder diffraction. $MnNbF_6$ undergoes a first order rhombohedral to cubic transition at ~315 K, but $ZnNbF_6$ is rhombohedral over the temperature range examined (~100 to 500 K). $MnNbF_6$ displays zero thermal expansion at ~380 K and NTE above this temperature. $MnNbF_6$ became completely rhombohedral on initial compression and transformed to an unidentified phase at ~ 6 GPa. Rhombohedral $MnNbF_6$ is initially elastically very soft (K_0 ~ 5 GPa), but stiffens considerably on compression. Below ~3.5 GPa it displays negative linear compressibility. $ZnNbF_6$ remained rhombohedral over the entire pressure range examined (0 - ~4 GPa) and displayed a similar stiffening on compression.

KEY WORDS: Negative thermal expansion; phase transition; metal fluoride; zero thermal expansion; negative linear compressibility.

1. INTRODUCTION

Since the 1996 report of negative thermal expansion (NTE) over a wide temperature range in ZrW_2O_8,[1-2] strong NTE has been observed in many different families of materials.[3-5] This interest in NTE has been partly motivated by a desire to control thermal expansion, using strategies such as the preparation of composites containing positive and negative thermal expansion phases.[6-7] When NTE materials are employed in composites they can experience significant stresses due to the thermal expansion mismatch between the NTE phase and the matrix. In the case of framework NTE materials, which often display structural phase transitions at low pressure, these stresses can degrade the performance of the composite. This motivates the study of such materials under pressure.

A wide variety of ReO_3-struture fluorides have received attention for their potential as negative and zero thermal expansion materials since the observation that cubic ScF_3 displays negative thermal expansion at all temperatures below ~1100 K.[8] With the correct choice of composition, fluorides displaying both negative thermal expansion and optical transparency from the mid-infrared through to the UV can be prepared.[9] A number of strategies for controlling thermal expansion in this type of material have explored, including the formation of solid solutions based on ScF_3,[10-13] an exploration of cation ordered $M^{II}M^{IV}F_6$[9, 14-16] notably including $CaZrF_6$[9] and $CaNbF_6$[15] which both display very strong NTE over a wide temperature range, the insertion of lithium,[17] and the introduction of excess fluoride to prepare ReO_3-related composition such as $Sc_{1-x}Zr_xF_{3+\delta}$,[18] $YbZrF_7$[19] and $TiZrF_{7-x}$.[14]

The current study builds up on prior examinations of $CaNbF_6$[15] and $MgNbF_6$,[15] to better understand how ReO_3-type $M^{(II)}NbF_6$ respond to compression and temperature changes as chemical composition is varied. $MnNbF_6$ and $ZnNbF_6$ were examined by synchrotron x-ray powder diffraction from 100- 500 K and upon compression to > 4 GPa. The synthesis, room temperature crystal structures and spectroscopic data for these two materials were reported by Chassaing and coworkers in 1982.[20] Magnetism and the magnetic structure of $MnNbF_6$ were reported in 1986,[21] and a synthesis and powder diffraction data for $ZnNbF_6$ were reported in 1998.[22]

2. EXPERIMENTAL

2.1. Syntheses

All syntheses were conducted in a dry nitrogen atmosphere, due to the moisture sensitivity of reagents. NbF_4 was prepared by solid state reaction of NbF_5 and niobium metal based on the procedures reported by Chassaing et al.[23] The reactants were ground together in a 5:1 molar ratio (NbF_5 to Nb), with excess Nb^{5+} needed to fully react with the Nb^0 according to Chassaing et al. The mixture was placed in a copper tube, which was sealed by arc-welding under argon. The copper tube was sealed in an evacuated fused silica am-

pule. The reaction vessel was heated to 300 °C, held there for 99 h, and then quenched to room temperature. A vacuum sublimation, using a rotary pump and a temperature of ~100 °C, was used to separate product from excess reactant. The result was a black hygroscopic powder.

$MnNbF_6$ and $ZnNbF_6$ were prepared by solid state reaction of NbF_4 and MF_2 (M=Mn, Zn). These syntheses were based on the work of Goubard et al.[22] The reactants were ground together in a 1:1 ratio and loaded into a copper tube, which was sealed by arc-welding under argon. The copper tube was then sealed in an evacuated fused silica ampule. The ampule was quickly heated to 520 °C, held there for approximately one week, and slowly cooled to room temperature. The resulting $MnNbF_6$ and $ZnNbF_6$ products were grey powders.

2.2. Variable Temperature X-ray Powder Diffraction Measurements

X-ray powder diffraction data were recorded on a Perkin-Elmer amorphous silicon 2D detector using a wavelength of 0.72950 Å at beamline 17-BM of the Advanced Photon Source, Argonne National Laboratory. An Oxford Cryostream was used to control the sample temperature between 100 and 500 K. As the indicated temperature does not necessarily represent the true sample temperature, calibration data was collected using a thermocouple inserted into an empty Kapton capillary. The difference between the temperature recorded on the thermocouple and that indicated by the Cryostream controller was used as a correction to estimate the true sample temperature for the diffraction experiments.

2.3. High Pressure X-ray Diffraction Measurements

High pressure powder x-ray diffraction data were collected on the 17-BM beamline at the Advanced Photon Source, Argonne National Laboratory. Data were recorded on a Perkin-Elmer amorphous silicon 2D detector, using a wavelength of 0.72768 Å. An EasyLab "Diacell Bragg-(G)" diamond anvil cell (DAC), equipped with a diaphragm so that the pressure could be automatically increased, was used. Silicone oil (Alfa, MW = 237 g·mol^{-1}) was used as the pressure medium. Pressure was determined from the lattice constant of NaCl, which was added as a pressure marker, using an equation of state reported by Birch.[24] Data were acquired while the pressure was continuously increased. Due to the pump program used and the non-linear relationship between pressure in the diaphragm and pressure in the sample chamber, the pressure increments associated with each frame of x-ray data are non-uniform.

2.4. Rietveld Analyses of the Powder Diffraction Data and the Calculation of Expansion Coefficients

All Rietveld refinements were performed using the General Structure Analysis System (GSAS)[25] and EXPGUI.[26] Examples of fit quality are given in the supplemental information. The unit cell volumes and temperatures were used to calculate coefficients of thermal expansion (CTEs). The variation of the volume CTE with temperature was estimated in two ways, by differentiating a multi-term (6 terms for $MnNbF_6$ and 4 terms for $ZnNbF_6$) polynomial fit to volume vs temperature and using a point by point approach.

3. RESULTS AND DISCUSSION

3.1. Thermal Expansion and Phase Behavior of $MnNbF_6$

Synchrotron x-ray powder data, Figure 1, recorded from 110 to 500 K show a first order phase transition from rhombohedral (R-3) to cubic (Fm-3m) at ~315 K in $MnNbF_6$ (see Fig. 1b). This transition has previously been reported to occur at 323 K.[21] While some ReO_3-type metal fluorides remain cubic on cooling, many display similar cubic to rhombohedral phase transitions.[15, 27-28] The observed transition involves correlated tilting of the MF_6 octahedra ($a^-a^-a^-$ type).[29]

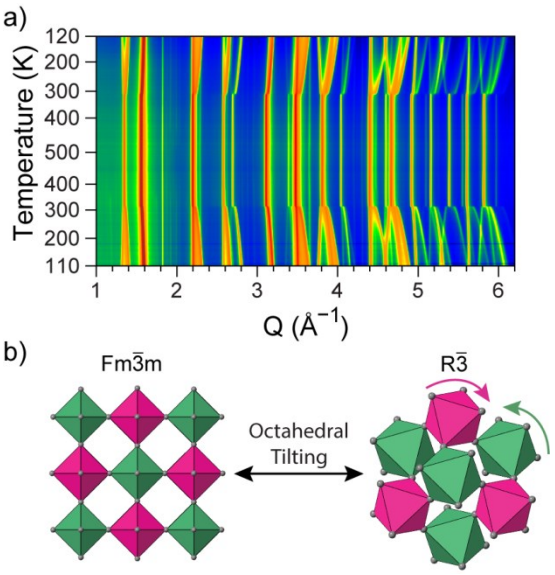

Figure 1: a) Synchrotron powder x-ray diffraction data as a function of temperature for $MnNbF_6$. There is a cubic to rhombohedral phase transition at ~ 315 K, b) which involves correlated octahedral tilts.

The volume per formula unit and volumetric CTE are shown in Figure 2. The rhombohedral phase shows a large increase in volume on heating, with α_v ~ 200 ppmK^{-1} from 110 - 200 K. This is typical of ReO_3-type metal fluorides.[15, 28] The increase in M-F-M bond angle on heating the rhombohedral phase more than compensates for any negative contribution to the CTE from transverse vibrations of the linking fluoride. The positive thermal expansion (PTE) increases on warming and becomes very large close to the phase transition as the octahedral tilt disappears and the material becomes cubic.

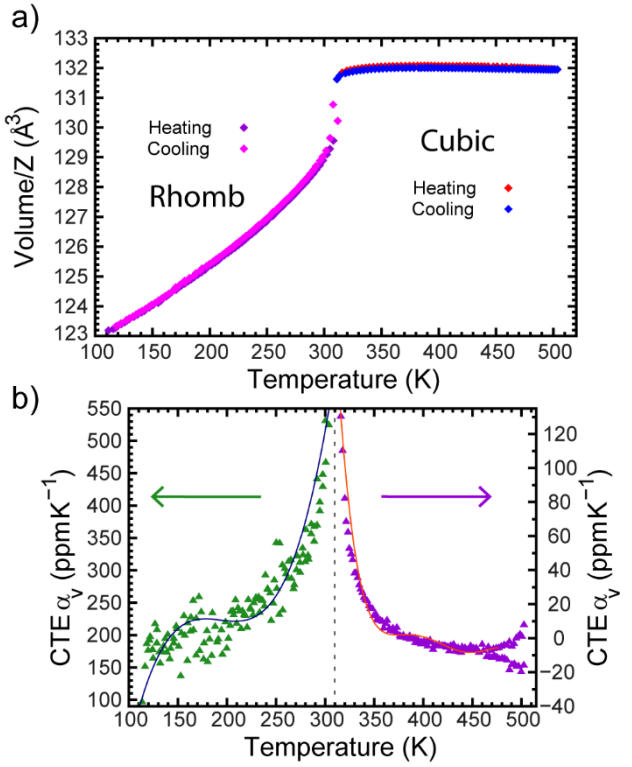

Figure 2: a) Volume per formula unit and b) volumetric coefficients of thermal expansion (CTE) determined from a 6 term polynomial fit (solid lines) and using a point by point method for $MnNbF_6$. Single phase Rietveld fits were used to determine the volumes, with a change from a rhombohedral to a cubic model at ~ 315 K.

Immediately above the transition temperature the cubic phase shows PTE, which changes through zero to weak NTE at higher temperatures; α_v of 0.0 ppmK^{-1} at 382 K, and α_v of ~ -6 ppmK^{-1} at 450 K. Above 450 K, the apparent CTEs on heating and cooling vary due to some hysteresis in the diffraction measurements. The origin of this behavior is unclear, but it may be an experimental artefact.

3.2. Thermal Expansion and Phase Behavior of $ZnNbF_6$

The response of $ZnNbF_6$ to changes in temperature was also probed by synchrotron x-ray powder diffraction. Unit cell volume and volumetric CTE versus temperature are shown in Figure 3. This sample adopted a rhombohedral (R-3) structure over the entire measured temperature range. Some apparent hysteresis is seen between the data recorded on heating and cooling, which is most likely an experimental artefact. As the experimentally determined unit cell volume varies smoothly on cooling, we believe that it most accurately represents the true sample behavior. The thermal expansion of $ZnNbF_6$, Figure 3b, is strongly positive, with a α_v of 107 ppmK^{-1} at 120 K. The CTE increases on further heating, with a α_v ~ 315 ppmK^{-1} at 499 K.

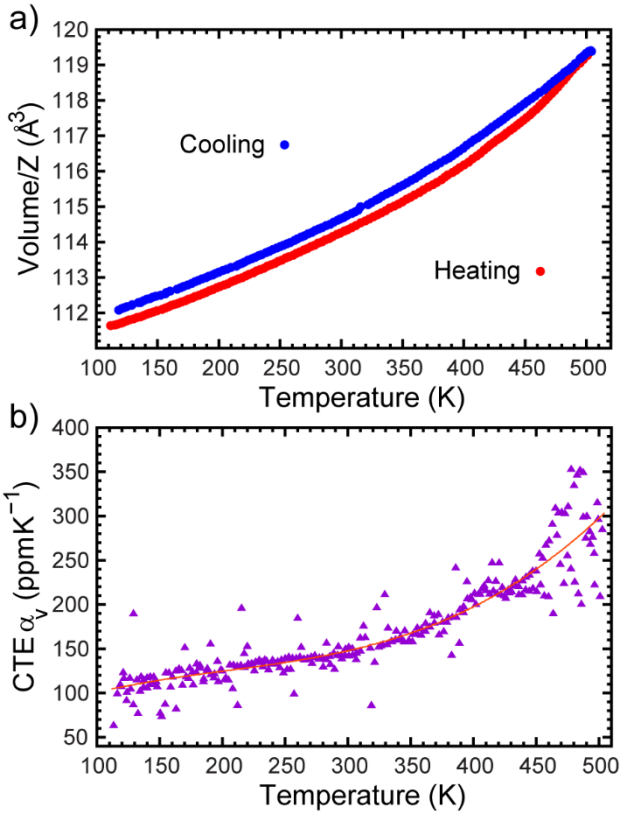

Figure 3: a) Volume per formula unit and b) volumetric coefficient of thermal expansion (CTE) determined from a 4 term polynomial fit (solid line) and using a point by point approach for $ZnNbF_6$ as determined from Rietveld fits of a rhombohedral (R-3) model to the variable temperature x-ray powder diffraction data.

The thermal expansion of several rhombohedral ReO_3–connectivity metal fluorides[11, 15-16, 30-31] are compared in Figure 4. The expansion of $MnNbF_6$ is similar to that of $MgNbF_6$, with a large positive CTE that increases dramatically close to the rhombohedral to cubic phase transition. The successive replacement of Mg by Mn and then Zn stabilizes the rhombohedral structure to increasingly higher temperatures. This is not purely a consequence of changes in ionic radii, as the six coordinate ions have Shannon effective radii of 72, 82 and 74 pm respectively.[32] It is likely related to an increase in the covalency of the bonding on moving from Mg to Zn, as highly ionic bonding stabilizes the maximum volume cubic structure[33] and Zn is significantly more electronegative than Mg (1.66 versus 1.23).[34] At the maximum temperature studied, $ZnNbF_6$ displays higher thermal expansion than InF_3 and AlF_3, which both remain rhombohedral to high temperatures (>650 K).[30-31]

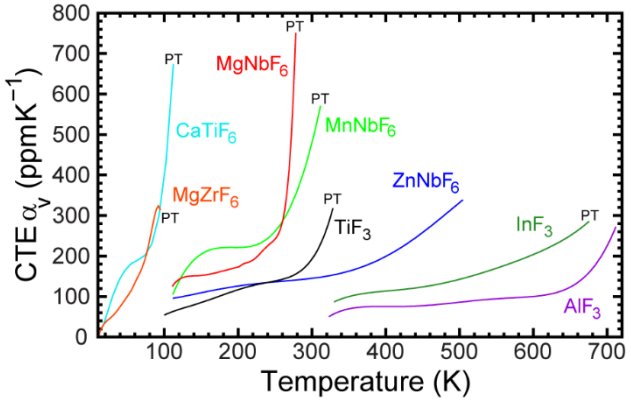

Figure 4: A comparison of the CTEs for rhombohedral ReO_3-type metal fluorides. The CTEs were estimated by differentiating six term polynomial fits to volume vs temperature.

3.3. Compression of $MnNbF_6$

The response of $MnNbF_6$ to compression was studied by variable pressure powder x-ray diffraction in a DAC. The resulting data are shown as a 2D-contour plot in Figure 5a. This plot shows evidence of a phase transition at very low pressure, associated with peak splitting indicative of octahedral tilting on compression, and a transition to a poorly ordered phase at ~6 GPa. Close inspection of the data reveals that the initial diffraction patterns show phase coexistence of rhombohedral and cubic phases. This is not unreasonable given the first order nature of the thermally induced transition and a transition temperature close to ambient. The phase coexistence persists during the first few frames of diffraction data, as there is a delay between the increase in methanol pressure supplied to the diaphragm on the DAC and any significant increase in the pressure experienced by the sample. An example Rietveld fit to data in this region is shown in Fig S5.

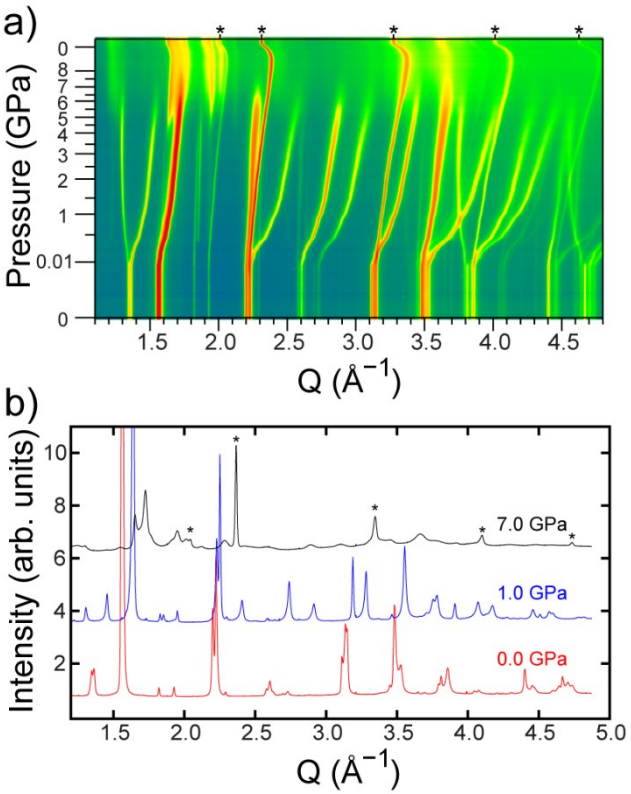

Figure 5: a) High pressure powder x-ray diffraction data for $MnNbF_6$ and b) selected powder diffraction patterns. Diffraction peaks from the NaCl internal pressure standard are marked by *.

As the pressure increases, the $MnNbF_6$ sample completely transforms to rhombohedral material. On further compression, the evolution of the data is consistent with increasing octahedral tilting in the R-3 phase. Above 6 GPa, the peaks from the rhombohedral phase disappear and broad peaks appear alongside those from NaCl indicating that $MnNbF_6$ transforms to a poorly ordered structure, Figure 5b. This behavior is distinct from that previously seen for $CaNbF_6$.[15] Unlike $MnNbF_6$, $CaNbF_6$ undergoes a transition from cubic Fm-3m to a poorly ordered phase at ~0.4 GPa. The reason for the difference is unclear.

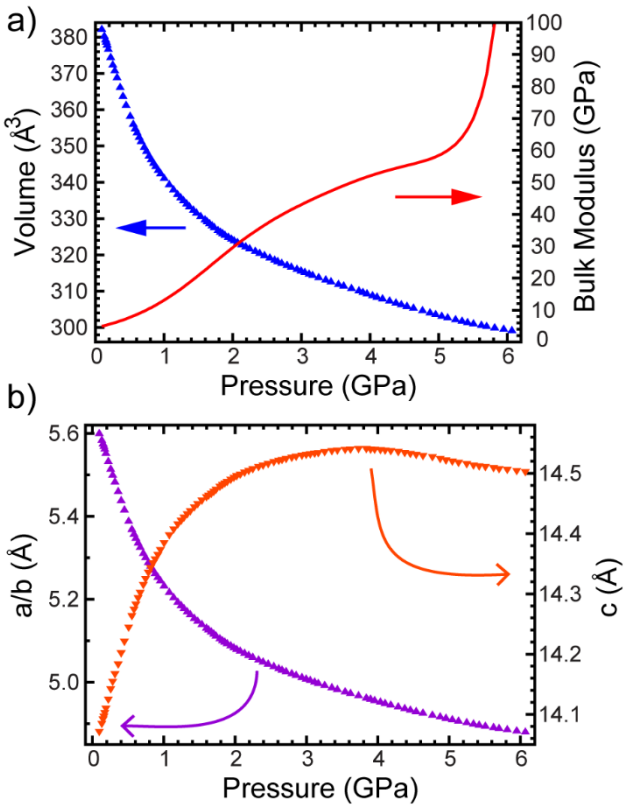

Figure 6: a) Unit cell volume, bulk modulus and b) lattice constants for $MnNbF_6$. Note the two y-axes are scaled differently.

Unit cell volume versus pressure for rhombohedral $MnNbF_6$ is shown in Figure 6a along with an estimate of how the bulk modulus evolves on compression. The later was calculated by differentiating a six term polynomial, which had been fit to ln(V) vs P. This approach was adopted as the V versus P data could not be fit satisfactorily using a conventional equation of state. At low pressures, the material is extremely soft. The bulk modulus increases from 5 to 12 GPa on compression to ~1 GPa. This contrasts with what is typically seen in cubic ReO_3-type metal fluorides, for example $CaNbF_6$ has $K_{0(298K)} = 33.7(4)$ GPa and displays pronounced softening on compression, $K'_{0(298\ K)} \sim -23(2)$, rather than stiffening. However, behavior of this type is to be expected for rhombohedral ReO_3-connectivity phases, as tilting of the framework octahedra (bending Mn-F-Nb links) initially provides a low energy path for volume reduction On compression above 1 GPa, the structure continues to stiffen with the bulk modulus exceeding 60 GPa prior to the transi-

tion to a poorly ordered phase. This stiffening presumably occurs because the pressure induced octahedral tilts bring the fluoride ions closer together. The compressibility of the rhombohedral phase is highly anisotropic (Fig. 6b); it displays negative linear compressibility parallel to the c-axis up to ~3.8 GPa, and it is elastically very soft in the a-b plane. This occurs because the octahedral tilts involve rotation around crystallographic 3-fold axes leading to a reduction in metal – metal separation in the a-b plane, and in parallel with this there is an octahedral distortion that leads to negative linear compressibility parallel to the c-axis.[16] Similar behavior has been seen in other rhombohedral ReO_3-type fluorides.[16, 35-36]

3.4. Compression of $ZnNbF_6$

The high pressure powder x-ray diffraction data for $ZnNbF_6$ are presented in Figure 7.

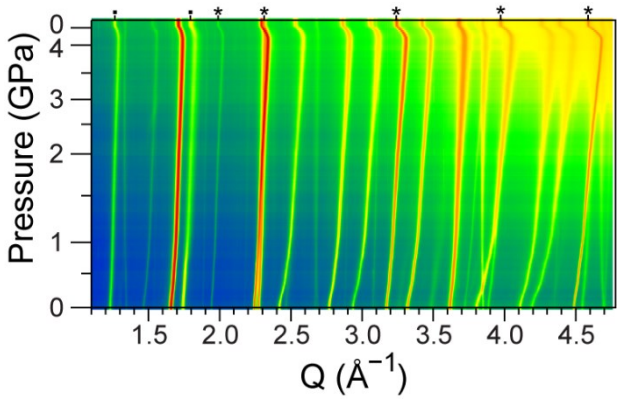

Figure 7: Diffraction data as a function of pressure for $ZnNbF_6$. Diffraction peaks from the internal pressure standard, NaCl, are marked with * and an impurity phase with ■. The sample was decompressed at the end of experiment.

The diffraction patterns evolve smoothly on increasing and decreasing pressure, without any additional peak splitting or new peaks indicating that $ZnNbF_6$ remains in the rhombohedral phase up to the highest pressures recorded, ~ 4 GPa. An additional minor phase, not seen in the variable temperature experiments for this sample, appears throughout these data. It seems likely that it formed while grinding the sample. Similar behavior has been seen in other ReO_3-type fluorides including $CaZrF_6$.[9]

An example Rietveld fit for rhombohedral $ZnNbF_6$ is given in Figure S7. Unit cell volumes and bulk moduli, calculated from a six term polynomial fit to ln(V) vs pressure, are shown in Figure 8. Similar to $MnNbF_6$, a conventional equation of state, such as Burch Murnaghan, did not give a satisfactory fit to the V versus P data. $ZnNbF_6$ is elastically soft at low pressures, with a bulk modulus of ~14 GPa at ambient. However, it stiffens rapidly on compression leading to a bulk modulus of > 50 GPa at pressures above 3.5 GPa. Similar to the Mn analog, the compressibility is highly anisotropic. The material is very soft in the a-b plane, but parallel to the c-axis it displays negative linear compressibility below 2.0 GPa (Figure 8b). The greater ambient pressure bulk modulus for $ZnNbF_6$ versus $MnNbF_6$ (~14 and ~5 GPa respectively) and the much smaller fractional increase in the c-axis on compression prior to the onset of positive linear compressibility parallel to the c-axis presumably reflects the considerable octahedral tilting that is already present in the $ZnNbF_6$ at ambient pressure and temperature (Zn-F-Nb angle is ~148.8(5)° at ambient pressure).

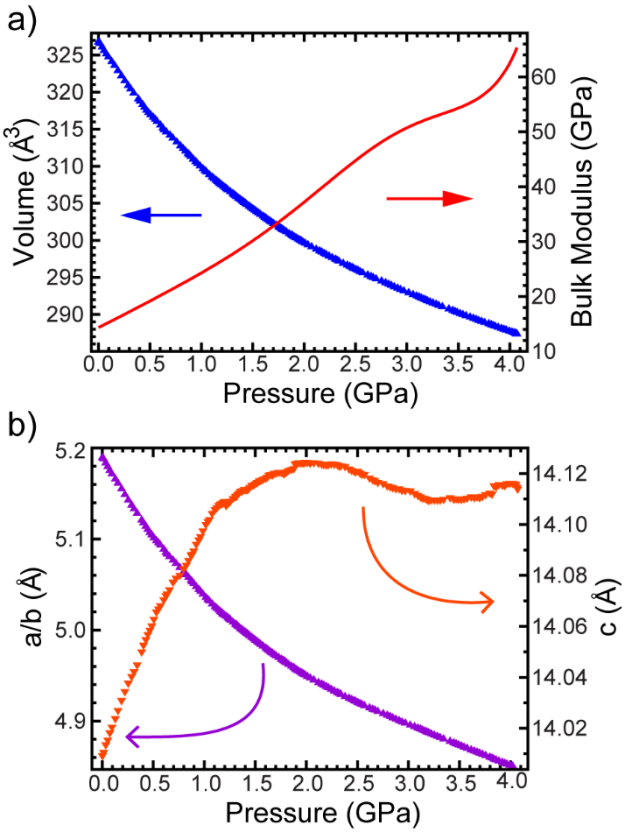

Figure 8: a) Unit cell volume, bulk modulus and b) lattice constants for $ZnNbF_6$. Note the two y-axes are scaled differently.

The compressibilities of $MnNbF_6$ and $ZnNbF_6$ are compared to those of some other ReO_3-related rhombohedral metal fluorides in Figure 9.[16, 35-36] The general trend in elastic stiffness (slope of V versus P) at ambient, or close to ambient pressure, reflects the trend in M-F-M' bond angles at close to ambient pressure. CrF_3, which has the smallest M-F-M angle (~144.8° at ambient), is the stiffest phase and $CaTiF_6$ is the softest with a Ca-F-Ti angle of 158.9° at 0.25 GPa.

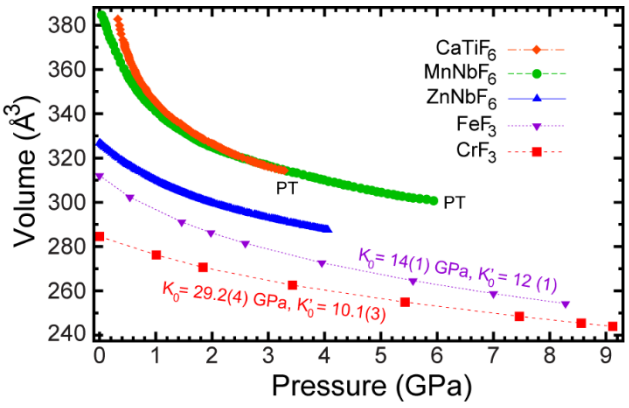

Figure 9: Unit cell volume versus pressure for several rhombohedral ReO_3-related fluorides.

4. CONCLUSIONS

The responses of ReO_3-type $ANbF_6$ (A = Ca, Mg, Mn and Zn) to changes in temperature and pressure are varied. $CaNbF_6$ has previously been reported to retain a cubic cation ordered structure over a wide temperature range (from less than 10 to at least 900 K).[15] However, $MgNbF_6$ and $MnNbF_6$ display rhombohedral to cubic transitions, involving the correlated titling or corner shared octahedral, on heating above ~280 and ~315 K respectively. Even though Zn^{2+} has a similar ionic radius to Mg^{2+}, $ZnNbF_6$ adopted a rhombohedral structure over the entire temperature rage investigated (~100 – 500 K). This is likely a consequence of zinc's greater electronegativity when compared to magnesium, as more ionic bonding is thought to favor the cubic phase.[33] The behavior of $CaNbF_6$ on compression is distinct from that of both $MnNbF_6$ and $ZnNbF_6$. $CaNbF_6$ transform from a cubic ReO_3 structure to a poorly ordered phase on compression to ~0.4 GPa.[15] However, both $MnNbF_6$ and $ZnNbF_6$ adopt rhombohedral ReO_3-type structures to quite high pressures (~6 GPa and > 4 GPa respectively). These rhombohedral phases are elastically very soft at close to ambient pressure, as the reduction of the M-F-Nb bond angles associated with tilting of the octahedra provides a low energy pathway for volume reduction, but they rapidly stiffen as the M-F-Nb bond angles are reduced due increasing steric repulsion.

ASSOCIATED CONTENT

Supporting Information. Example Rietveld fits, lattice constants versus temperature and pressure. This material is available free of charge via the Internet at http://pubs.acs.org.

AUTHOR INFORMATION

Corresponding Author

* E-mail: angus.wilkinson@chemistry.gatech.edu

ORCID

Angus P. Wilkinson: 0000-0003-2904-400X

Notes

The authors declare no competing financial interest.

ACKNOWLEDGEMENT

We are grateful for useful discussions with Ross Angel. The activities at Georgia Tech were supported in part under NSF DMR-1607316. This work made use of the Advanced Photon Source, a U.S. Department of Energy (DOE) Office of Science User Facility operated for the DOE Office of Science by Argonne National Laboratory under contract DE-AC02-06CH11357.

REFERENCES

1. Evans, J. S. O.; Mary, T. A.; Vogt, T.; Subramanian, M. A.; Sleight, A. W., Negative Thermal Expansion in ZrW_2O_8 and HfW_2O_8. *Chem. Mater.* **1996,** *8*, 2809-2823.

2. Mary, T. A.; Evans, J. S. O.; Vogt, T.; Sleight, A. W., Negative Thermal Expansion from 0.3 to 1050 Kelvin in ZrW_2O_8. *Science* **1996,** *272*, 90-92.

3. Lind, C., Two Decades of Negative Thermal Expansion Research: Where Do We Stand? *Materials* **2012,** *5* (6), 1125-1154.

4. Chen, J.; Hu, L.; Deng, J.; Xing, X., Negative thermal expansion in functional materials: controllable thermal expansion by chemical modifications. *Chem. Soc. Rev.* **2015,** *44* (11), 3522-3567.

5. Fisher, D. J., *Negative Thermal Expansion Materials*. Materials Research Foundations: 2018; Vol. 22, p 178.

6. Takenaka, K., Negative thermal expansion materials: technological key for control of thermal expansion. *Sci. Technol. Adv. Mater.* **2012,** *13* (1).

7. Takenaka, K., Progress of Research in Negative Thermal Expansion Materials: Paradigm Shift in the Control of Thermal Expansion. *Frontiers in Chemistry* **2018,** *6*, 267.

8. Greve, B. K.; Martin, K. L.; Lee, P. L.; Chupas, P. J.; Chapman, K. W.; Wilkinson, A. P., Pronounced Negative Thermal Expansion from a Simple Structure: Cubic ScF_3. *J. Am. Chem. Soc.* **2010,** *132* (44), 15496-15498.

9. Hancock, J. C.; Chapman, K. W.; Halder, G. J.; Morelock, C. R.; Kaplan, B. S.; Gallington, L. C.; Bongiomo, A.; Han, C.; Zhou, S.; Wilkinson, A. P., Large negative thermal expansion and anomalous behavior on compression in cubic ReO_3-type $A^{II}B^{IV}F_6$: $CaZrF_6$ and $CaHfF_6$. *Chem. Mater.* **2015**.

10. Morelock, C. R.; Greve, B. K.; Gallington, L. C.; Chapman, K. W.; Wilkinson, A. P., Negative Thermal Expansion and Compressibility of $Sc_{1-x}Y_xF_3$ ($x < 0.25$). *J. Appl. Phys.* **2013,** *114*, 213501.

11. Morelock, C. R.; Gallington, L. C.; Wilkinson, A. P., Evolution of Negative Thermal Expansion and Phase Transitions in $Sc_{1-x}Ti_xF_3$. *Chem. Mater.* **2014,** *26* (5), 1936-1940.

12. Morelock, C. R.; Gallington, L. C.; Wilkinson, A. P., Solid Solubility, Phase Transitions, Thermal Expansion, and Compressibility in $Sc_{1-x}Al_xF_3$. *J. Solid State Chem.* **2015,** *222*, 96-102.

13. Hu, L.; Chen, J.; Fan, L.; Ren, Y.; Rong, Y.; Pan, Z.; Deng, J.; Yu, R.; Xing, X., Zero Thermal Expansion and Ferromagnetism in Cubic $Sc_{1-x}M_xF_3$ (M = Ga, Fe) over a Wide Temperature Range. *J. Am. Chem. Soc.* **2014,** *136* (39), 13566-13569.

14. Yang, C.; Zhang, Y.; Bai, J.; Qu, B.; Tong, P.; Wang, M.; Lin, J.; Zhang, R.; Tong, H.; Wu, Y.; Song, W.; Sun, Y., Crossover of thermal expansion from positive to negative by removing the excess fluorines in cubic ReO_3-type $TiZrF_{7-x}$. *J. Mater. Chem. C* **2018,** *6* (19), 5148-5152.

15. Hester, B. R.; Hancock, J. C.; Lapidus, S. H.; Wilkinson, A. P., Composition, Response to Pressure, and Negative Thermal Expansion in $M^{II}B^{IV}F_6$ (M = Ca, Mg; B = Zr, Nb). *Chem. Mater.* **2017,** *29* (2), 823-831.

16. Hester, B. R.; Wilkinson, A. P., Negative Thermal Expansion, Response to Pressure and Phase Transitions in $CaTiF_6$. *Inorg. Chem. in press.*

17. Chen, J.; Gao, Q.; Sanson, A.; Jiang, X.; Huang, Q.; Carnera, A.; Rodriguez, C. G.; Olivi, L.; Wang, L.; Hu, L.; Lin, K.; Ren, Y.; Lin, Z.; Wang, C.; Gu, L.; Deng, J.; Attfield, J. P.; Xing, X., Tunable Thermal Expansion in Framework Materials through Redox Intercalation. *Nature Commun.* **2017,** *8*, 14441.

18. Wang, T.; Xu, J.; Hu, L.; Wang, W.; Huang, R.; Han, F.; Pan, Z.; Deng, J.; Ren, Y.; Li, L.; Chen, J.; Xing, X., Tunable Thermal Expansion and Magnetism in Zr-Doped ScF_3. *Appl. Phys. Lett.* **2016,** *109* (18), 181901.

19. Ticknor, J. O.; Hester, B. R.; Adkins, J. W.; Xu, W.; Yakovenko, A. A.; Wilkinson, A. P., Zero Thermal Expansion and Abrupt Amorphization on Compression in Anion Excess ReO_3-Type Cubic $YbZrF_7$. *Chem. Mater.* **2018**.

20. Chassaing, J.; Monteil, C.; Bizot, D., Crystallochemical and Spectroscopic Study of Fluoroniobates $MNbF_6$ with M = Mg, Ca, Fe, Co, Ni, Zn and Cd. *J. Solid State Chem.* **1982,** *43* (3), 327-333.

21. Bizot, D.; Chassaing, J.; Pannetier, J.; Leblanc, M.; Lebail, A.; Ferey, G., Fluorcomplexes of Niobium IV. 5. The Magnetgic-Structure of $MnNbF_6$. *Solid State Commun.* **1986,** *58* (1), 71-74.

22. Goubard, F.; Llorente, S.; Gaubicher, J.; Bizot, D.; Chassaing, J., Powder diffraction data for fluorocomplexes of niobium IV: $MNbF_6$ (M=Ca, Mg, Cd, Zn). *Powder Diffraction* **1998,** *13* (03), 163-165.

23. Chassaing, J.; Bizot, D., Synthesis, Spectroscopic and Magnetic Study of NbF_4. *J. Fluor. Chem.* **1980,** *16* (5), 451-459.

24. Birch, F., Equation of State and Thermodynamic Parameters of Sodium Chloride to 300 kbar in the High-Temperature Domain. *J. Geophys. Res. B* **1986,** *91* (B5), 4949-4954.

25. Larson, A. C.; Von Dreele, R. B., *GSAS - General Structure Analysis System*. Report LA-UR-86-748: Los Alamos Laboratory, 1987.

26. Toby, B. H., EXPGUI, a graphical user interface for GSAS. *J. Appl. Crystallogr.* **2001,** *34*, 210-213.

27. Daniel, P.; Bulou, A.; Rousseau, M.; Nouet, J.; Leblanc, M., Raman-Scattering Study of Crystallized MF_3 Compounds (M = Al, Cr, Ga, V, Fe, In) - An Approach to the Short-Range-Order Force-Constants. *Phys. Rev. B* **1990,** *42* (16), 10545-10552.

28. Hu, L.; Chen, J.; Xu, J.; Wang, N.; Han, F.; Ren, Y.; Pan, Z.; Rong, Y.; Huang, R.; Deng, J.; Li, L.; Xing, X., Atomic Linkage Flexibility Tuned Isotropic Negative, Zero, and Positive Thermal Expansion in $MZrF_6$ (M = Ca, Mn, Fe, Co, Ni, and Zn). *J. Am. Chem. Soc.* **2016,** *138* (44), 14530-14533.

29. Howard, C. J.; Kennedy, B. J.; Woodward, P. M., Ordered double perovskites - a group-theoretical analysis. *Acta Crystallogr., Sect. B* **2003,** *59*, 463-471.

30. Morelock, C. R. Thermal Expansion, Compressibility, and Local Structure of Fluorides and Oxyfluorides with the Rhenium Trioxide Structure. PhD Thesis, Georgia Institute of Technology, 2014.

31. Morelock, C. R.; Hancock, J. C.; Wilkinson, A. P., Thermal expansion and phase transitions of α-AlF_3. *J. Solid State Chem.* **2014,** *219*, 143-147.

32. Shannon, R. D.; Prewitt, C. T., Effective Ionic Radii in Oxides and Fluorides. *Acta Crystallogr., Sect. B* **1969,** *25*, 925-946.

33. Herzig, P.; Zemann, J., AB_3 Nets built from Corner-Connected Octahedra - Geometries, Electrostatic Lattice Energies, and Sterochemical Discussion. *Z. Krist.* **1993,** *205*, 85-97.

34. Little, E. J.; Jones, M. M., A complete table of electronegativities. *J. Chem. Ed.* **1960,** *37* (5), 231.

35. Jorgensen, J. E.; Marshall, W. G.; Smith, R. I., The compression mechanism of CrF_3. *Acta Crystallogr., Sect. B* **2004,** *60*, 669-673.

36. Jorgensen, J. E.; Smith, R. I., On the compression mechanism of FeF_3. *Acta Crystallogr., Sect. B* **2006,** *62*, 987-992.